Journal of Materials Research and Technology 38 (2025) 276–287

Contents lists available at ScienceDirect

Journal of Materials Research and Technology

journal homepage: www.elsevier.com/locate/jmrt

Evaluation of shear strength and interlayer damage of short carbon fiber reinforced PA6 in FDM printing along critical ZX orientation

Selim Hartomacıoğlu [a,b,*], Paşa Yayla [c], Şakir Yazman [d], Salih Dağlı [e], Murat Sarıkaya [e,f]

[a] Department of Mechanical Engineering, Marmara University, 34854, Istanbul, Türkiye
[b] Department of Mechanical Engineering, Recep Tayyip Erdoğan University, Rize, 53100, Türkiye
[c] Engineering Faculty, Mechanical Engineering Department, Marmara University, Maltepe, 34854, Istanbul, Türkiye
[d] Ilgın Vocational School, Selçuk University, 42615, Konya, Türkiye
[e] Department of Mechanical Engineering, Sinop University, Sinop, Türkiye
[f] Faculty of Mechanical Engineering, Opole University of Technology, 45-758, Opole, Poland

A R T I C L E I N F O

Handling editor: SN Monteiro

Keywords:
Fused deposition modeling
Short carbon fiber
Polyamide 6
Shear strength
Interlayer bonding
Finite element analysis
Damage analysis

A B S T R A C T

This study experimentally and numerically investigates the shear strength and interlayer damage mechanisms of short carbon fiber-reinforced Polyamide 6 (PA6-CF15) composites fabricated via Fused Deposition Modeling (FDM) along the critical ZX build orientation. Using a Taguchi experimental design, the effects of key processing parameters—nozzle temperature, layer thickness, number of outer walls, and post-heat treatment duration—on shear strength were systematically analyzed. Experimental results indicated that PA6-CF15 specimens exhibited higher maximum shear loads compared to neat PA6, although they demonstrated more brittle behavior and lower ductility, primarily due to insufficient fiber bridging in the Z-direction. The optimal parameters for maximizing shear strength were identified as a nozzle temperature of 260 °C, a layer thickness of 0.15 mm, two outer walls, and 80 min of post-heat treatment. Finite Element Analysis (FEA) corroborated experimental findings by revealing stress concentrations near shear notch regions and confirming that optimized parameters enhance interlayer cohesion. Furthermore, comprehensive surface roughness measurements and Scanning Electron Microscopy (SEM) analyses provided detailed insights into damage progression. Higher nozzle temperatures and thinner layers resulted in smoother surfaces and denser structures, which correlated with improved shear strength. SEM images revealed complex failure mechanisms including fiber-matrix debonding, fiber pullout, matrix cracking, and fiber breakage, with evidence of matrix smearing and ductile drawing. The finite element simulations predicted a maximum shear stress of 151.6 MPa and an average shear stress of 23.4 MPa under optimized conditions, aligning well with experimental observations. Among the examined parameters, layer thickness had the most pronounced influence on shear strength, followed by wall line count and heat treatment duration, while nozzle temperature exhibited a comparatively moderate effect. The findings underscore the critical role of process parameter optimization in enhancing the shear strength and overall mechanical performance of FDM-printed short carbon fiber-reinforced PA6 composites, offering valuable guidance for both academic research and industrial applications.

1. Introduction

Additive manufacturing (AM) technology has become an important alternative in the industry by offering flexibility and cost advantages in production processes. In particular, the Fused Deposition Modeling (FDM) technique is widely preferred due to its low-cost and easy-to-apply method. However, the mechanical properties of parts produced with the FDM method vary depending on the production direction. This situation can negatively affect the durability of the products due to the weakness of the interlayer bonding. For this reason, the use of composite materials to increase the mechanical performance of parts produced with FDM is becoming increasingly common. Thermoplastic matrix

* Corresponding author. Department of Mechanical Engineering, Recep Tayyip Erdoğan University, Rize, 53100, Türkiye.
E-mail addresses: selimh@marmara.edu.tr (S. Hartomacıoğlu), pasa.yayla@marmara.edu.tr (P. Yayla), syazman@selcuk.edu.tr (Ş. Yazman), sdagli@sinop.edu.tr (S. Dağlı), msarikaya@sinop.edu.tr (M. Sarıkaya).

https://doi.org/10.1016/j.jmrt.2025.07.220
Received 23 June 2025; Received in revised form 21 July 2025; Accepted 24 July 2025
Available online 26 July 2025

composites reinforced with reinforcements such as carbon fiber, glass fiber and Kevlar are the focus of research in this area.

Recent studies primarily focus on the manufacturing and characterization of fiber-reinforced composites as FDM-printed components, which successfully address the limitation of poor mechanical characteristics in the printed parts [1–5]. At present, fiber reinforced thermoplastic composites used as FDM printing feedstock are classified into two categories: 1) short fiber reinforced thermoplastics (SFRT) and 2) continuous fiber reinforced thermoplastic composites (CFRT). FDM printing of CFRT provides a substantial enhancement in mechanical qualities, suitable for use in aircraft as structural components. Conversely, FDM of SFRT has significant promise in the automotive sector because of its lightweight honeycomb structures and cost-effectiveness. Polymers are modified with continuous or short fibers to create fiber-reinforced polymers (FRP) [6]. Fiber-reinforced polymers combine lightweight polymer matrices with stiff, strong fibers to provide exceptional processability, wear resistance, and a high strength-to-weight ratio.

Polyamide 6 (PA6), a semi-crystalline polymer, has superior processing capability and formability, coupled with exceptional corrosion and wear resistance, making it an optimal selection for a polymer matrix [7]. Peng et al. [8] a PA6–carbon fiber (CF) composite filament for FDM printing and demonstrated that the strength and modulus of FDM-printed PA6-CF specimens consistently increase as porosity (void content) decreases with increasing build-plate temperature. Sun et al. [6] sought to improve the performance of 3D-printed PA6-CF composite materials by modifying carbon fiber content, optimizing printing settings, and improving heat treatment conditions. Results demonstrated that under ideal processing circumstances, the maximum tensile strength of the PA6-CF composite material was 162 MPa, signifying a 406 % enhancement relative to pure PA6 material. Rashid et al. [9] conducted experimental research on the influence of infill patterns and densities on the mechanical performance of additively built carbon fiber-reinforced PA6 composites. Sandwich constructions with various core configurations (such as triangular, hexagonal, and rectangular) and infill densities (ranging from 18 % to 62 %) were constructed. Triangular and hexagonal infill designs exhibited superior performance at reduced infill densities, but rectangular infill patterns offered enhanced mechanical strength and elongation at elevated infill densities.

Cho et al. [10] improved the PA6-CF composite by interfacial reinforcement with a combination of adhesive and reduced-graphene oxide coating. The altered composite composition demonstrated a 73 % enhancement in flexural strength and an 84 % improvement in modulus. Lupone et al. [11] employed FDM to fabricate carbon fiber-reinforced PA6 composites, varying the raster angle in the layer sequence based on distinct manufacturing designs. Subsequently, laser writing was executed to create electrical pathways on the surfaces of the printed components. Moreover, decreasing fiber content or integrating plasticizers improved the toughness of the composite material. Toro et al. [12] established that augmenting the fiber content in carbon fiber-reinforced PA6 composites (10–30 %) led to a rise in internal porosity and enhanced mechanical characteristics. Li et el [7]. fabricated PA6-CF composites containing up to 35 % carbon fiber with a dedicated screw extrusion 3D printer. As a result, at 25 % CF content, the tensile strength was approximately 170 MPa, was approximately 220 % higher than that of unfilled PA6. Long fiber preservation and low porosity contributed to the high mechanical strength. Zhang et al. [13] used a designed FDM 3D printer with ultrasonic deposition to enhance the interfacial adhesion between hot melt glass fiber and PA6. The researchers reported that as the ultrasound frequency increased, the porosity decreased from 4.52 % to 1.33 % and the mechanical properties improved. They also claimed that this method solved the interfacial bonding problem of fiber-reinforced polymers with FDM 3D printing. Du et al. [14] emphasized that the mechanical properties of carbon fiber reinforced PA6 composites depend largely on the fiber-matrix interface and showed that up to 20 % increase in tensile strength was achieved by improving this interface through surface treatments. Bai et al. [15] produced continuous carbon fiber reinforced PA6 rods by thermoplastic pultrusion method and examined the effect of drawing speed on surface quality, void ratio and mechanical properties; the lowest void ratio (0.7 %) and the highest surface quality were obtained at low drawing speed. Li et al. [16] examined the long-term interfacial performance of a pultruded unidirectional carbon/glass hybrid rod under water immersion and hydraulic pressure, showing that while water exposure led to a gradual decline in interfacial shear strength, the presence of hydraulic pressure helped mitigate this degradation, particularly in the outer glass fiber shell. Recent work by Xian et al. [17] demonstrated that temperature cycling significantly accelerates interfacial shear strength degradation in carbon/glass hybrid rods, while smaller diameters and random fiber distribution offer better long-term durability under environmental exposure.

Table 1
Mechanical properties of filaments.

Properties	Unit	PA6	PA6-CF15
Printed Part Density (dry)	kg/m^3	1115–1050	1203
Melting Temperature	°C	195–197	234
Glass Transition Temperature	°C	49	70
Tensile Strength	MPa	16.4–17.6	18.2–19.1
Elongation at Break	%	0.8–12.8	0.5–0.8
Young Modulus	MPa	2122–334	3532–2455
Impact Strength Izod (Unnotched)	kJ/m2	3.2–17.4	2.9–4.1

As can be understood from the literature review, studies on fiber-reinforced thermoplastic composites produced by FDM method have generally focused on basic mechanical properties such as tensile and flexural strength. However, shear strength, which is of critical importance especially in industrial applications, has been addressed in a limited number of studies. This situation reveals the need for research to improve the interlayer bonding performance of composite materials produced by FDM.

In this study, shear strength of short carbon fiber-reinforced PA6 materials produced by FDM method and layer bonding in ZY direction was experimentally investigated. The effects of production parameters (i.e., nozzle temperature, layer thickness, number of outer walls and post-heat treatment time) on shear strength were analyzed in detail and optimal production conditions were determined. In addition, fracture mechanisms were evaluated with SEM analyses and surface roughness measurements performed after production, providing a comprehensive view of material performance.

One of the novelty aspects of the study is the optimization of the results obtained by using Taguchi experimental design method and finite element analysis (FEA) and systematic analysis of the effects of production parameters on shear strength. With this approach, it is aimed to improve the mechanical performance of composites produced by FDM method and to develop suggestions for industrial applications.

As a result, this study aims to fill an important gap in the literature and to provide valuable contributions to both academic and industrial fields by providing guiding information for increasing the shear strength of short carbon fiber reinforced PA6 composites produced by FDM.

2. Material and method

In this study, carbon fiber-reinforced polyamide 6 (PA6-CF15) filaments with a diameter of 1.75 mm, commercially supplied by BASF, were used as feedstock. These filaments consist of 15 wt% short carbon fibers embedded in a PA6 matrix. Table 1 presents the key mechanical and thermal properties of the unfilled PA6 and the reinforced PA6-CF15 materials used to fabricate the specimens in the ZX build orientation, where interlayer bonding is typically most critical.

To reduce the cost and complexity associated with full factorial testing, the experimental matrix was designed using the Taguchi method, a statistical approach widely utilized for parameter

Table 2
Test parameters and their levels.

	Factor	Unit	Level 1	Level 2	Level 3
A	Nozzle Temperature	°C	245	260	275
B	Layer Thickness	mm	0.15	0.30	0.45
C	Wall Line Count	Number	0	1	2
D	Heat Treatment Time	Min	0	80	160

Table 3
Fixed printing parameters.

Parameter	Unit	Value
Initial Layer Height	mm	0.25
Infill Density	%	100
Infill Pattern		Lines
Build Plate Temperature	°C	100
Flow Rate	%	100
Print Speed	mm/s	40
Regular Fan Speed	%	0

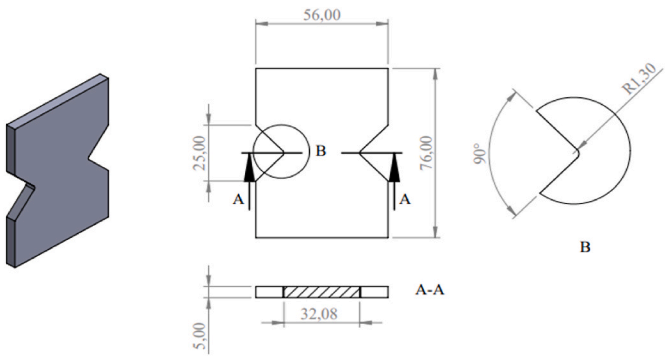

Fig. 1. Details of the shear test specimen.

optimization in engineering studies. This methodology enables efficient identification of significant factors and their interactions while minimizing the number of required experiments.

Four process parameters were selected based on literature review and preliminary investigations: nozzle temperature, layer thickness, number of outer walls, and post-printing heat treatment duration. Among these, nozzle temperature and layer thickness are well-documented as critical factors influencing mechanical performance. The nozzle temperature range was determined according to the manufacturer's specifications for the carbon fiber-reinforced PA6 filament, ensuring optimal thermal behavior during extrusion. The selected layer thickness levels (0.15 mm, 0.30 mm, and 0.45 mm) correspond to 25–75 % of the 0.6 mm nozzle diameter, representing practical and widely adopted values for FDM printing. The number of outer walls is a less frequently explored parameter despite its potential impact on the structural integrity of printed parts. Although two outer walls are generally recommended in standard FDM practices, no systematic investigation has addressed its effect on shear performance. Therefore, three levels (0, 1, and 2) were examined. For the post-print heat treatment, a fixed temperature of 150 °C was selected based on prior successful applications in the literature. Xu et al. [18] demonstrated that post-heat treatment of carbon fiber-reinforced nylon at 140–160 °C significantly improved interlaminar shear strength. Motivated by this, three durations (0, 80, and 160 min) were applied to evaluate the time-dependent influence on interlayer bonding and crystallinity.

Accordingly, in this study, process parameters including nozzle temperature, layer thickness, number of outer walls, and post-heat treatment time at 150 °C were systematically varied, as detailed in Table 2.

A full factorial design with four factors at three levels each would require 81 experimental runs. However, using the Taguchi L9 orthogonal array, the number of unique experiments was reduced to 9, each repeated three times, resulting in 27 tests in total.

All specimens were fabricated using an Ultimaker S5 3D printer, which features a dual extrusion system and a build volume of 330 × 254 × 300 mm^3. A 0.6 mm nozzle was used, and the filaments were dried at 60 °C for 12 h prior to printing to eliminate moisture-induced defects. Fixed printing parameters are listed in Table 3.

The shear test specimens were designed according to ASTM D7078 and printed in the ZX direction to promote interlayer loading. The specimen geometry is illustrated in Fig. 1, while Fig. 2 provides visual documentation of the printer setup, nozzle system, and build orientation.

After fabrication, each specimen was weighed using a precision analytical balance, and surface roughness was measured with a Keyence digital optical microscope. Mechanical testing was carried out on a Shimadzu universal testing machine using a custom-developed pure shear test fixture. The test setup and apparatus are shown in Fig. 3.

Shear stress and strain were calculated using the following equations:

$$\tau_{xy} = \frac{F}{A};\ \Upsilon_{xy} = \frac{\Delta_x}{l} \tag{1}$$

where F represents the load applied, A the cross-section area between the notches, Δ_x the displacement, and l is the initial length. The values of the shear modulus (G) of polymeric composites have been defined from the slope of the shear stress-strain curves by means of Eq. (2):

$$G = \frac{\tau_{xy}}{\Upsilon_{xy}} = \frac{Fl}{A.\Delta_x} \tag{2}$$

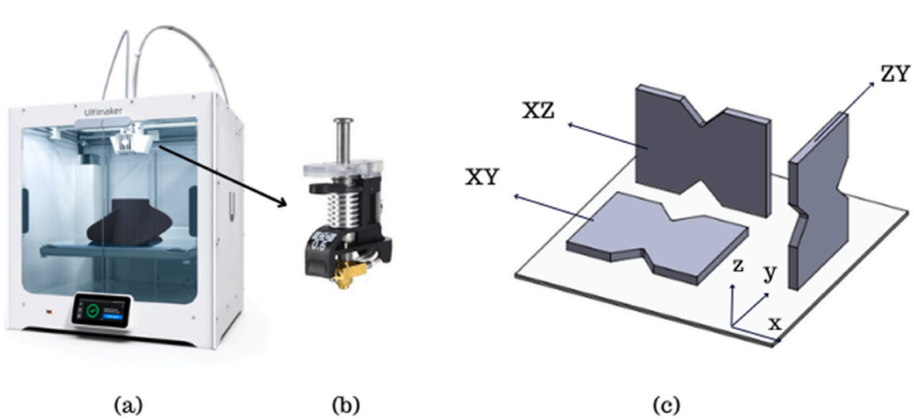

Fig. 2. a) 3D Printer, b) Heat core, c) Build orientation.

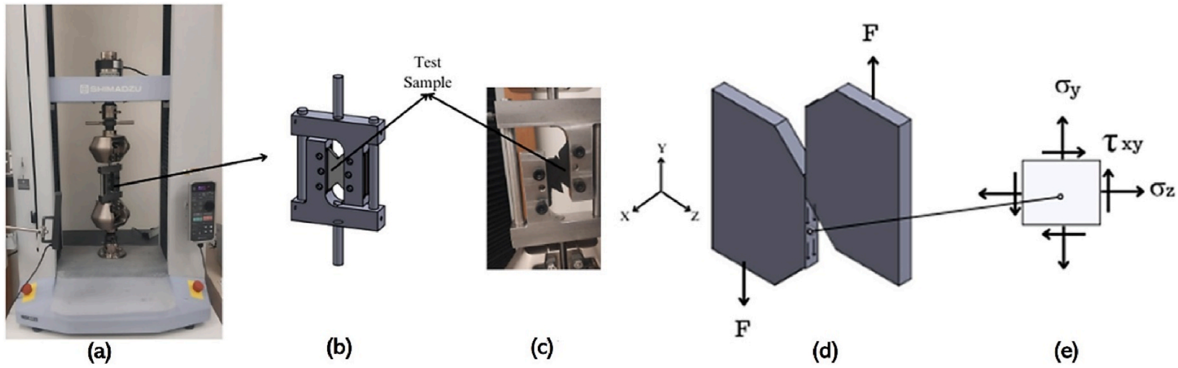

Fig. 3. Shear test setup.

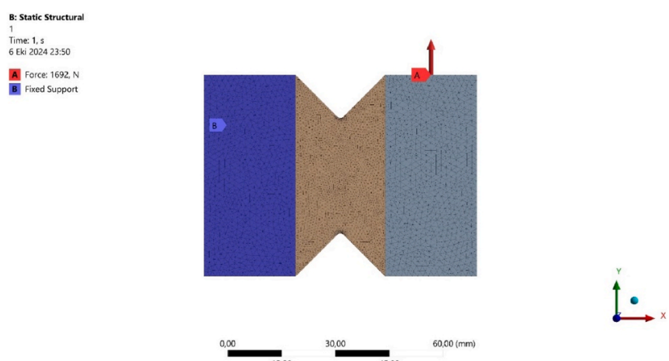

Fig. 4. Load and boundary conditions of FEA study.

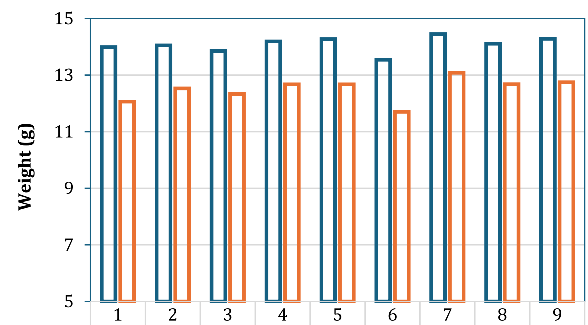

	1	2	3	4	5	6	7	8	9
PA6 +CF15	13.99	14.05	13.85	14.19	14.27	13.54	14.45	14.11	14.28
Pure PA6	12.06	12.53	12.33	12.67	12.67	11.7	13.08	12.68	12.75

Fig. 5. Weight results.

Experimental results were analyzed using the Taguchi method to determine the signal-to-noise (S/N) ratios for each factor. Additionally, full-factorial estimates for the 81 possible configurations were generated, and three-dimensional surface plots were developed to visualize the influence of each parameter.

Finite Element Analysis (FEA) was conducted using ANSYS Static Structural to simulate the stress distribution observed during shear testing. Mesh refinement was applied to regions of interest, particularly around the notched areas. Load and boundary conditions mirrored those used in physical testing and are presented in Fig. 4. The simulation yielded insights into equivalent stress distributions, shear-line stress profiles, and potential failure zones.

Finally, fracture surface analysis was performed using both macro and micro-scale imaging techniques. Macrostructural observations were obtained using a Keyence VHX-900F optical microscope, while microstructural features and failure modes were investigated via SEM using a Hitachi SU-1510. These analyses provided a detailed understanding of damage progression and failure mechanisms in the printed composites.

3. Results and discussion

3.1. Weight

Weight variation among the fabricated samples provides crucial insight into the internal structure and material deposition efficiency, particularly in fiber-reinforced composites fabricated via FDM. In this study, the weights of PA6 and PA6-CF15 specimens were measured to investigate the influence of selected processing parameters on part density and material distribution. As reported in prior research, process parameters such as nozzle temperature, layer thickness, and wall line count significantly influence material flow, fusion quality, and void formation, all of which directly affect the final weight of the printed components [19–21].

As illustrated in Fig. 5, the sample produced under the 7th experimental condition exhibited the highest recorded weight. This particular configuration involved a nozzle temperature of 275 °C, a minimal layer thickness of 0.15 mm, two outer walls, and a post-heat treatment duration of 80 min. The elevated nozzle temperature likely enhanced the thermal energy available for filament melting, thereby improving interlayer bonding and reducing porosity. This is consistent with literature findings, where higher nozzle temperatures have been shown to yield more homogeneous deposition, better fusion, and ultimately denser structures [22,23].

Additionally, a reduced layer thickness contributes to an increased number of deposited layers, enhancing bonding opportunities and limiting void formation. The presence of two outer walls further contributed to the weight increase by introducing additional material to the periphery of each specimen. The application of heat treatment for 80 min may also have supported post-deposition diffusion and reorganization of polymer chains, potentially enhancing interlayer adhesion and reducing residual stresses, further contributing to overall densification.

Conversely, the lowest weight was recorded for the 6th experiment, which featured a nozzle temperature of 260 °C and zero outer walls. In this scenario, the combination of sub-optimal thermal input and the absence of reinforcing outer perimeters likely led to incomplete fusion and increased internal porosity, resulting in a lightweight structure. Lower nozzle temperatures are known to reduce melt viscosity and wetting capability, thereby impairing layer fusion and interfacial bonding [24].

Taken together, these findings confirm that higher nozzle temperatures, reduced layer thicknesses, increased wall line count, and moderate post-heat treatment durations favor a denser and heavier final structure. On the other hand, reduced thermal energy and structural minimalism—such as omitting outer walls—result in lower mass, likely

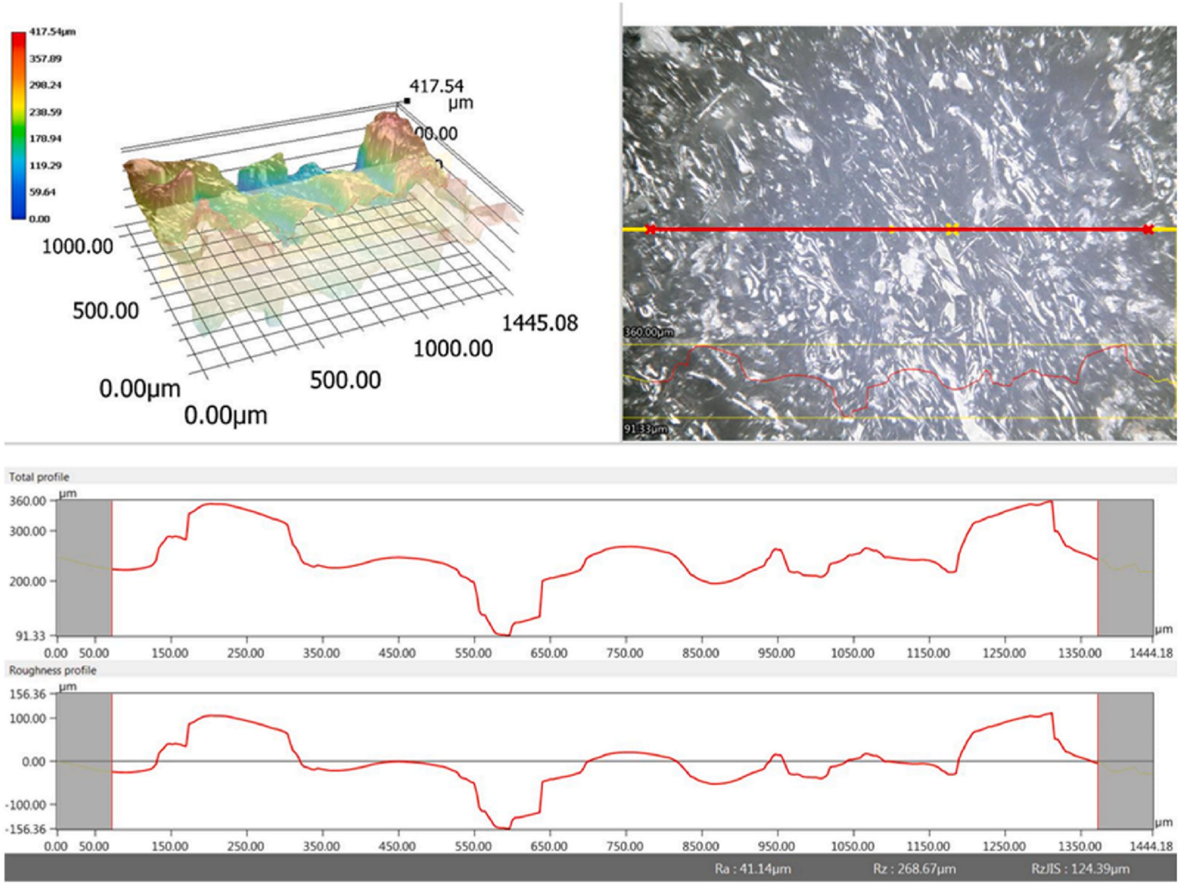

Fig. 6. 3D topography image obtained from the slip line and roughness distribution.

due to a higher prevalence of voids and poor interlayer connectivity. This outcome underlines the importance of process optimization in tailoring the physical properties of FDM-fabricated fiber-reinforced composites.

3.2. Surface roughness

Surface roughness is a critical parameter that significantly influences the functional performance of parts produced by AM, particularly in fiber-reinforced polymer composites. In FDM, surface quality directly affects mechanical performance, tribological behavior, and the initiation and propagation of cracks under stress. Roughness features—especially those formed along interlayer boundaries—are often considered precursors to localized failure in polymer-based components [1,25]. In particular, abrupt surface transitions at interlayer zones can lead to stress concentrations under shear loading, which accelerate crack initiation and compromise mechanical integrity. This effect is especially pronounced in the ZX build orientation, where the loading direction is perpendicular to the layer planes. Therefore, minimizing surface roughness is not only beneficial for dimensional accuracy but also plays a critical role in reducing local stress risers and improving the structural reliability of FDM-printed composites.

In this study, the effect of processing parameters on surface morphology was investigated using three roughness metrics: total height (Rt), arithmetic average roughness (Ra), and average peak-to-valley height (Rz). These metrics provide quantitative insight into the quality of the printed surface, particularly along the shear line where mechanical failure is most likely to initiate. Surface roughness measurements were performed using a non-contact optical method based on 3D surface topography analysis. A Keyence VHX-900F digital optical microscope equipped with a 50 × objective lens was utilized to scan the central shear region of each specimen. The scanned area was approximately 1.5 mm × 1.0 mm, and the vertical axis captured height variations up to ~1000 μm, corresponding to the Rt values. This technique allowed for high-resolution, contact-free surface profiling, enabling accurate quantification of surface roughness without introducing mechanical artifacts.

Table 4
Surface roughness results (Rt, Ra and Rz).

Exp. No	Rt	Ra	Rz
1	417.54	41.14	268.67
2	369.21	34.59	173.88
3	422.22	67.57	277.13
4	283.70	26.80	166.10
5	292.25	41.50	219.92
6	678.44	148.11	499.18
7	222.16	32.89	140.77
8	568.15	64.80	287.19
9	469.05	43.56	194.05

Fig. 6 illustrates a representative 3D topography image and the associated surface roughness profile acquired along the shear region. Quantitative roughness results for all experimental conditions are presented in Table 4. Among the tested parameters, Rt is especially critical for damage analysis, as it indicates the vertical distance between the highest peak and the lowest valley on the surface—a potential zone of stress concentration during mechanical loading [25,26].

The results show a clear correlation between surface roughness and processing conditions. Notably, the 6th experimental condition yielded the highest surface roughness values (Rt = 678.44 μm, Ra = 148.11 μm, Rz = 499.18 μm). This sample was fabricated using a moderate nozzle temperature (260 °C), a thick layer (0.45 mm), and no external wall lines. These parameters likely reduced interlayer bonding and surface

Table 5
Maximum shear load (in N) and average shear strength values (in MPa) obtained from experimental tests on PA6 and PA6-CF15 specimens.

Experiment No	PA6-CF15 *(N)*	Av. Shear Stregth of PA6CF15 [MPa]	PA6 *(N)*	Av. Shear Stregth of PA6 [MPa]
1	1990.37	12.43	1914.69	11.96
2	2402.68	15.02	2152.84	13.45
3	1606.87	10.05	1561.29	9.75
4	2176.85	13.60	2197.47	13.73
5	2431.21	15.20	2215.89	13.84
6	1520.69	9.50	3069.83	19.18
7	**3001.44**	**18.76**	**3118.76**	**13.24**
8	1802.13	11.26	1482.91	9.26
9	1346.80	8.41	Fault	–

Note: Bold values represent the highest load recorded for each material across all configurations. Missing PA6 data were not available for those specific tests due to limitations during specimen preparation or testing.

integrity, leading to prominent ridges and valleys. Coincidentally, this sample also exhibited lower shear strength and reduced weight, suggesting that insufficient thermal fusion and material deposition adversely impacted both structural and surface characteristics.

Conversely, the 7th experiment yielded the lowest surface roughness (Rt = 222.16 μm, Ra = 32.89 μm, Rz = 140.77 μm). In this configuration, a higher nozzle temperature (275 °C), thinner layer thickness (0.15 mm), and two external walls were employed, along with post-heat treatment. This combination likely enhanced the uniformity of material deposition and improved interfacial diffusion, resulting in smoother surface morphology. The same sample also exhibited the highest shear strength and weight values, which reinforces the intrinsic link between surface smoothness and overall mechanical performance.

These findings are consistent with the literature, which suggests that higher surface roughness facilitates microcrack formation, increases localized stress concentrations, and accelerates mechanical failure under shear or tensile loads [27–29]. On the other hand, smoother surfaces tend to distribute stress more evenly, enhance contact interfaces, and mitigate premature damage.

In summary, this study confirms that surface roughness—especially Rt—is a strong indicator of part quality and mechanical reliability. Optimizing FDM processing parameters to reduce surface irregularities is thus essential for enhancing both the structural integrity and durability of fiber-reinforced thermoplastic composites.

3.3. Shear strength

Shear strength is a critical indicator of interlayer bonding quality in FDM, especially for functional and load-shear strength composite components. In FDM, where parts are formed layer-by-layer, weak interlayer adhesion often limits structural integrity. Therefore, understanding how different process parameters affect shear performance is essential for improving the reliability of 3D-printed composites. In this study, the shear performance of PA6-CF15 was experimentally and numerically investigated, and the results were further supported by Taguchi statistical analysis and full-factorial prediction.

3.3.1. Experimental trials

The maximum shear load values for both PA6 and PA6-CF15 specimens under different experimental conditions are summarized in Table 5. As expected, PA6-CF15 specimens consistently outperformed pure PA6 across all configurations. The highest shear load for PA6-CF15 was obtained in Experiment 7 (3001.44 N), and the highest shear load for PA6 was obtained in Experiment 7 (3118.76). These findings align with the literature, where short fiber-reinforced thermoplastics demonstrate significant enhancements in interlayer mechanical performance due to fiber bridging and stress redistribution mechanisms [4,9]. However, in this study, the results differed due to the specimens being

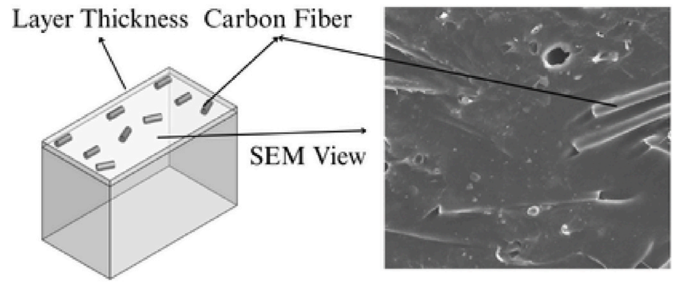

Fig. 7. Schematic representation and SEM micrograph of carbon fiber reinforced FDM-printed specimen in the ZX orientation.

printed in the ZX orientation, which is critical because of poor interlayer bonding and limited fiber bridging along the build orientation. Fig. 7 shows that the microstructure contains voids, fiber-matrix debonding, and shear-induced fiber ship marks, as revealed by SEM analysis. The observations indicate that the carbon fibers are mostly oriented within individual layers and fail to establish connections across the interlayer boundaries. Consequently, there is no fiber bridging in the build (Z) direction, which is critical for enhancing interlayer strength. The lack of fiber continuity between layers results in poor interfacial bonding and reduces the expected mechanical reinforcement effect. Thus, despite incorporating carbon fibers, the overall improvement in mechanical properties remains limited due to insufficient fiber interaction in the layer-stacking direction.

On the other hand, the lowest load for PA6-CF15 was observed in Experiment 9 (1346.80 N), correlating with a higher layer thickness (0.45 mm) and absence of post-processing. The variability in performance across samples demonstrates the critical role of FDM parameters in tuning shear strength. In contrast to our study focusing on the critical ZX orientation, Hartomacıoğlu et al. [30] demonstrated that carbon fiber-reinforced PA6 components fabricated in horizontal orientations can achieve significant mechanical performance gains when combined with optimized generative design and FDM parameters.

The shear test results presented in Fig. 8 indicate a distinct difference in ductility and toughness between PA6-CF15 and neat PA6 specimens. While PA6-CF15 samples exhibited higher maximum force values in most experiments, they fractured at significantly lower stroke values, suggesting limited plastic deformation and brittle-like behavior. In contrast, neat PA6 specimens demonstrate extended stroke capacities, with several samples (e.g., Exp. 6 and Exp. 7) reaching beyond 20 mm, indicative of superior ductility. Despite their lower peak force, PA6 samples were able to absorb more energy over the course of deformation, highlighting their tougher mechanical response under shear loading. This contrast suggests that the addition of short carbon fibers increases stiffness and strength but may compromise interlayer bonding in the ZX orientation, resulting in premature failure and reduced overall toughness. The absence of fiber bridging between layers appears to limit the reinforcing effect of the fibers, especially under high-displacement shear conditions.

3.3.2. Finite Element Analysis (FEA)

Due to the geometry of the test specimen, stress concentration occurs at the onset of the shear path. Analytical calculations of average shear stress do not account for this localized peak. In reality, this region experiences significantly higher stresses, which influence the overall shear response. Therefore, in this study, Finite Element Analysis (FEA) was employed to more accurately capture local stress distributions, and FEA results were used throughout the optimization process.

To further understand the stress distribution and failure mechanisms, FEA simulations were conducted using experimentally obtained maximum loads as inputs. Fig. 9 displays simulation results for Experiment 2, showing the maximum shear stress, average shear stress, equivalent (von Mises) stress, and total deformation distributions. These

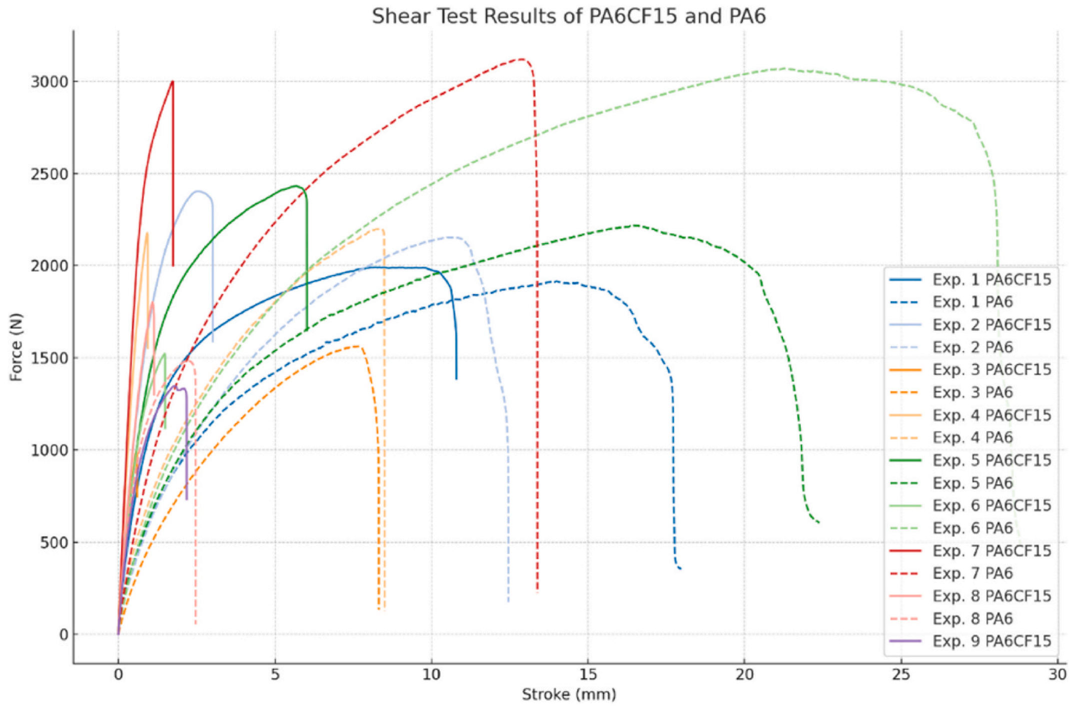

Fig. 8. Shear test results.

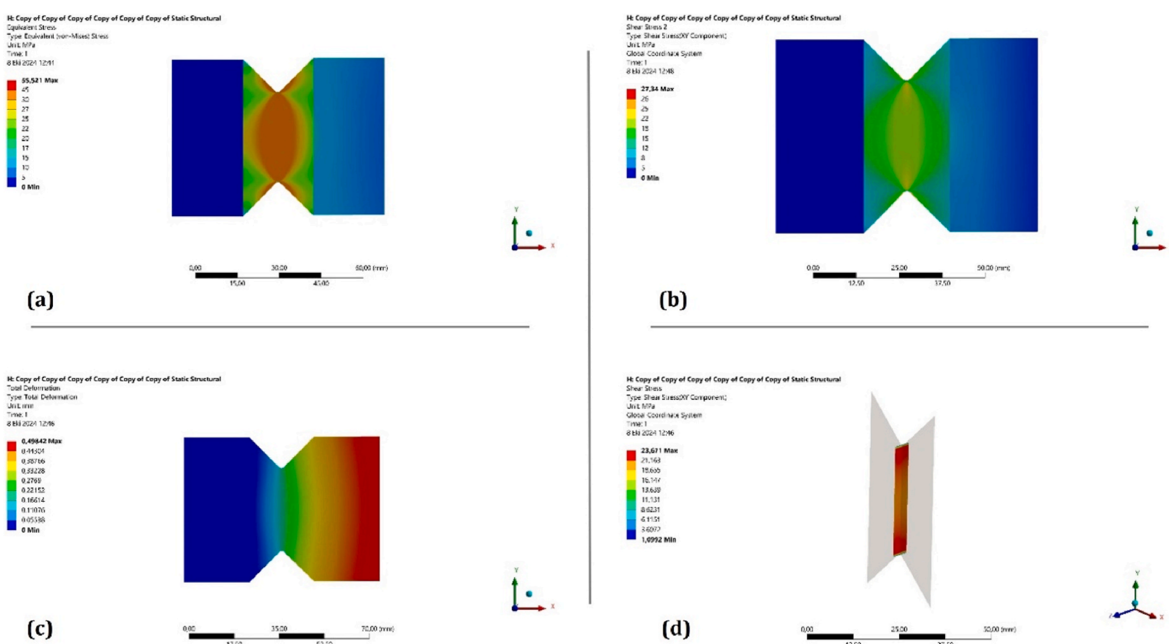

Fig. 9. FEA results for Experiment 2 showing: (a) maximum shear stress, (b) average shear stress, (c) von Mises stress, and (d) total deformation.

visualizations clearly indicate stress concentration near the shear notch regions, a common failure site in layered composites.

The shear stress distribution along 40 predefined nodes on the shear line was extracted and plotted in Fig. 10. This high-resolution mapping reveals localized variations that are likely governed by microstructural heterogeneities and voids introduced during printing. In Fig. 11, a comparison of maximum and average shear stresses is presented for each configuration. Notably, Experiment 7 yielded the highest maximum shear stress of 151.6 MPa, and an average shear stress of 23.4 MPa, confirming its superior interlayer cohesion.

These results support prior studies [20,31,32], which have shown that increased printing temperature, reduced layer thickness, and optimized post-processing led to better filament fusion and mechanical interlocking, thus increasing both tensile and shear strengths.

Fig. 12 illustrates the comparison between experimental and FEA-based shear strength values for PA6-CF15 specimens. Due to stress concentration at the onset of the shear zone—caused by specimen geometry—analytical calculations tend to underestimate the true shear response. To account for this effect, FEA was utilized to compute more realistic shear strength values based on local stress distributions. The comparison confirms that FEA better captures the influence of geometric factors on shear behavior.

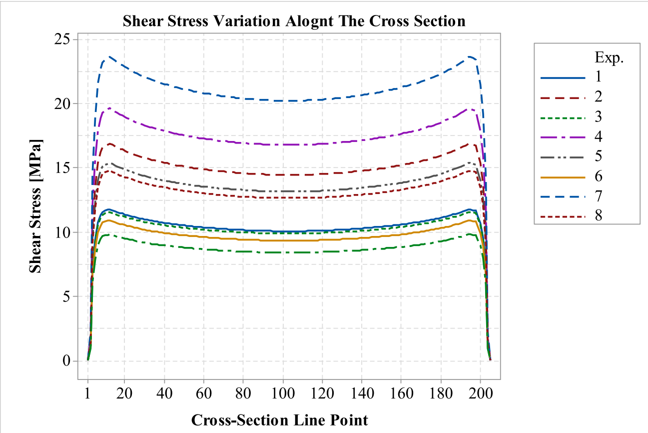

Fig. 10. Distribution of shear stress along the defined shear line (40-node sampling).

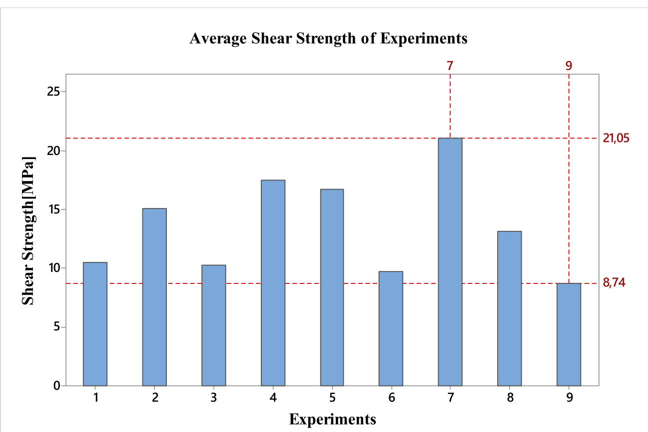

Fig. 11. Comparison of average and maximum shear stress values across tested configurations.

3.3.3. Taguchi-based optimization

The effects of individual process parameters were further investigated using the Taguchi method. The S/N ratio values for each experiment are illustrated in Fig. 13. Among the four factors studied, layer thickness (Factor B) had the most prominent effect: increasing thickness resulted in a marked decrease in S/N ratio, indicating a detrimental impact on shear strength. This is consistent with findings in literature, where larger layer heights are associated with weaker interlayer fusion and increased void content [1].

In contrast, outer wall count (Factor C) and heat treatment duration (Factor D) showed a positive contribution to shear strength at higher levels, likely due to enhanced surface integrity and improved polymer chain mobility. Based on S/N optimization, the optimal process parameters were determined as A2B1C3D2—corresponding to a nozzle temperature of 260 °C, a layer thickness of 0.15 mm, two outer walls, and 80 min of post-heat treatment.

3.3.4. Full-factorial prediction and statistical evaluation

To expand the design space beyond the experimental L9 array, 81 configurations were simulated using Taguchi estimation formulas. The

Fig. 13. Signal-to-noise (S/N) ratio chart for different FDM parameters based on Taguchi analysis.

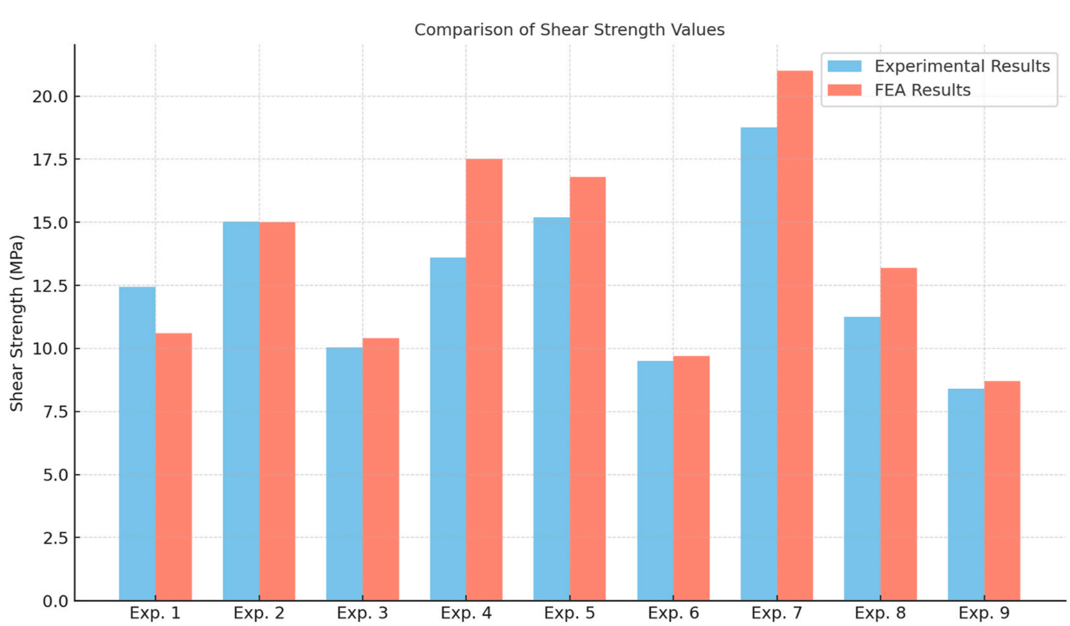

Fig. 12. Comparison of experimental and FEA shear strength results.

Table 6
Descriptive statistics of predicted shear strength values for 81 parameter combinations.

Variable	N	Mean	SE Mean	StDev	Min.	Q1	Median	Q3	Max.
Shear Strength	81	13.62	0.44	3.99	3.71	10.74	13.99	16.57	21.36

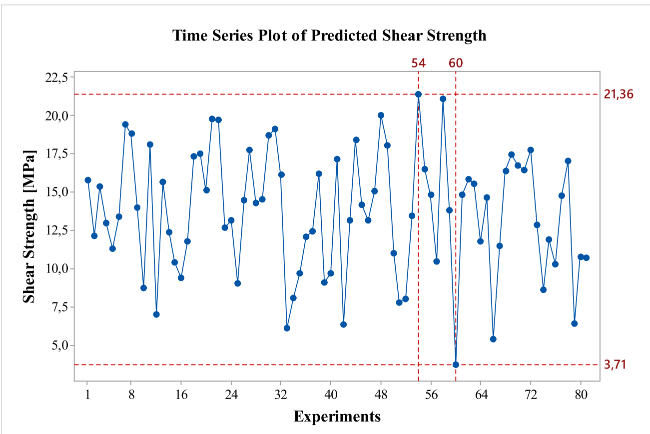

Fig. 14. Predicted shear strength values across all experimental configurations.

predicted shear strength values were statistically analyzed, and the results are presented in Table 6. The highest predicted shear strength was 21.36 MPa (54th configuration), while the lowest was 3.71 MPa (60th configuration). The mean shear strength across all predictions was 13.62 MPa, with a standard deviation of 3.99 MPa, indicating significant sensitivity to parameter changes.

The predicted values and their distribution are visualized in Fig. 14, and the interaction plots in Fig. 15 reveal synergistic effects between parameters. For example, thinner layers (0.15 mm) combined with higher nozzle temperatures (≥260 °C) and post-heat treatment consistently yielded superior shear strength, even when wall count was low. This interaction aligns with prior research indicating that thermal energy and part geometry co-determine bonding effectiveness in thermoplastics [8].

3.4. Damage analysis

To evaluate the failure mechanisms associated with shear loading, post-fracture surfaces of PA6-CF15 specimens were examined using Scanning Electron Microscopy (SEM) at multiple magnifications. The damage morphologies observed under varying nozzle temperatures and wall counts are shown in Fig. 16. These images provide insight into the structural evolution of damage zones and the micro-mechanical response of fiber-reinforced composites under interlayer shear loading.

At lower nozzle temperatures (245 °C and 260 °C), the extruder width (EW) boundaries—regions where the extruded filament interfaces with adjacent paths—appeared narrow and sharply defined (Fig. 16a and b). In contrast, specimens produced at the highest nozzle temperature (275 °C) displayed broadened EW zones with a more homogeneous and fused morphology (Fig. 16c). This suggests enhanced diffusion and wetting during deposition, likely facilitated by increased polymer chain mobility and fiber bridging between adjacent EW zones, as also noted in prior studies on thermoplastic fusion enhancement [33].

The geometry and continuity of EW boundaries significantly influenced the damage distribution across the shear planes. SEM analysis revealed that the extent and morphology of shear-induced damage zones varied according to the quality of interfacial bonding within these regions. In general, a combination of fiber–matrix debonding, fiber pull-out, matrix cracking, and fiber breakage was observed, with damage types often coexisting within the same specimen.

At early stages of shear deformation, void initiation and interfacial debonding were commonly observed near fiber–matrix interfaces, particularly in poorly fused zones. As the applied load increased, these deboned regions expanded via viscoelastic matrix deformation and plastic strain accumulation, eventually leading to fiber pullout phenomena (Fig. 16d). In regions subjected to higher local stresses, full fiber breakage occurred, especially where the fiber density was higher and mutual restriction of movement induced stress amplification (Fig. 16k and l).

Notably, shear-aligned fibers often showed evidence of relative

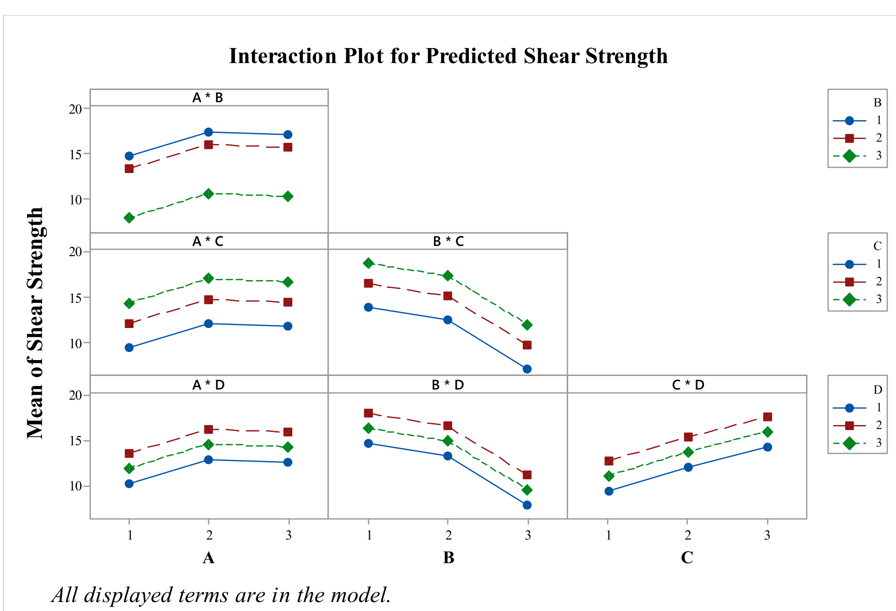

Fig. 15. Two-factor interaction plots for shear strength prediction.

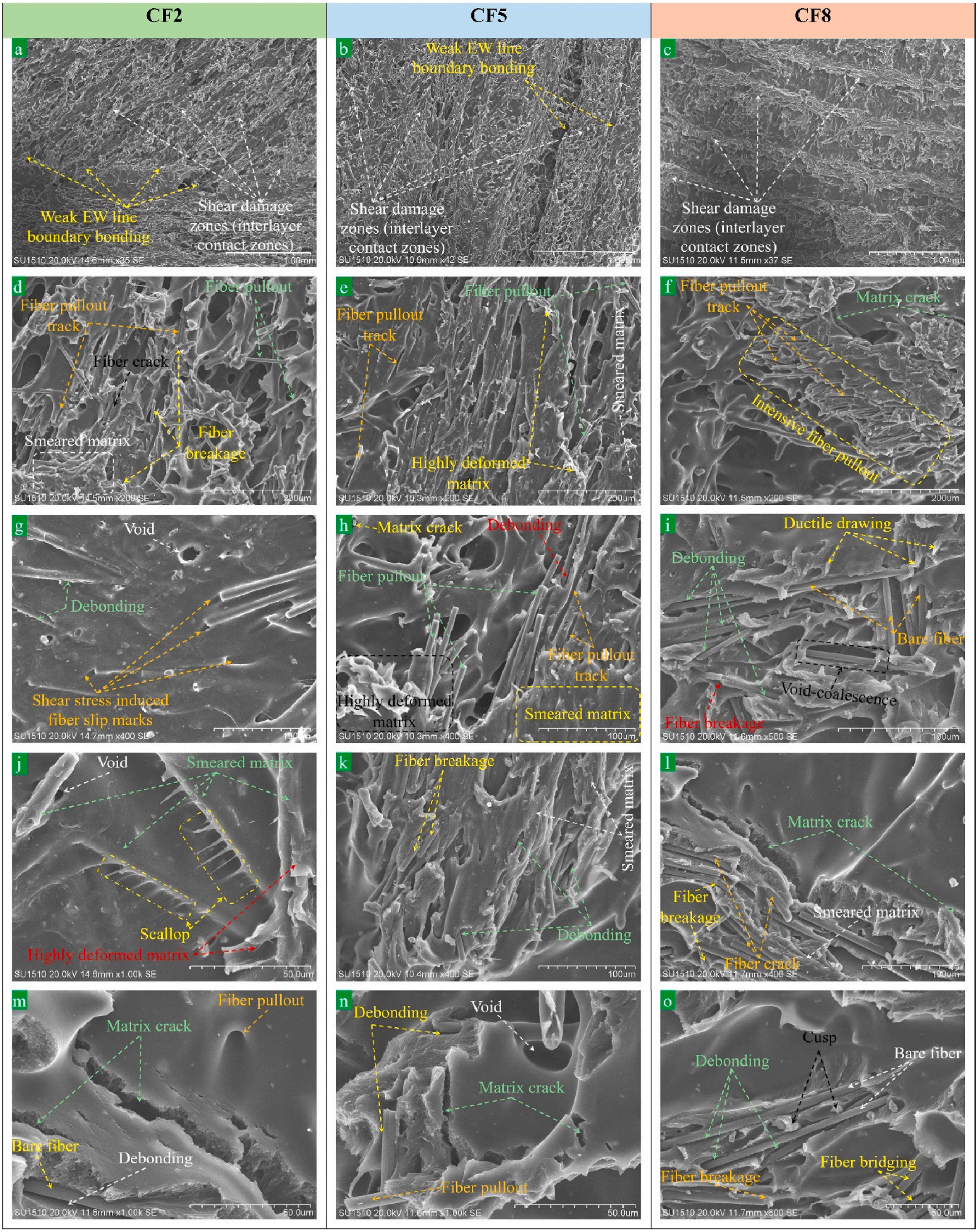

Fig. 16. SEM images of fracture surfaces from PA6-CF15 specimens produced at different nozzle temperatures and wall counts, showing diverse damage morphologies including (a–c) extruder width boundaries, (d–f) fiber pullout and breakage, (g) shear slip marks, (j) matrix smearing and scalloping, (k–l) cusp regions, (i, o) ductile drawing and bare fiber exposure, and (o) fiber bridging across matrix cracks.

sliding, leaving visible shear tracks along the direction of load application (Fig. 16g). This behavior supports the hypothesis that shear failure in FDM-printed composites is largely governed by interfacial shear stress rather than axial tensile loading [34,35].

Interestingly, fibers oriented transversely or obliquely to the shear direction were frequently observed to have smeared matrix layers on their trailing surfaces. These layers formed scallop-like patterns, indicating partial matrix yielding and adhesion failure during fiber sliding (Fig. 16j). These features suggest that matrix ductility plays a significant role in energy dissipation, particularly in high-toughness thermoplastic systems.

Additional morphologies such as cusp formation, matrix fibrillation, and ductile drawing were also prominent in regions of high deformation (Fig. 16i and o). These damage signatures are consistent with ductile fracture modes reported in the literature for fiber-reinforced thermoplastics [36–38]. Ductile drawing was particularly prominent between densely packed fiber clusters where matrix volume was low, resulting in nearly bare fibers visible on the fracture surface due to extensive matrix withdrawal (Fig. 16i).

Moreover, crack-bridging mechanisms were frequently observed in areas with favorable fiber orientation, suggesting that fibers significantly contributed to crack deflection and propagation retardation (Fig. 16o). This mechanism is essential in delaying catastrophic failure and is widely acknowledged as a major contributor to toughness in composite systems [39–41].

In summary, the SEM investigation highlights the complex interplay between process parameters, fiber orientation, and matrix behavior in determining the failure mechanisms of FDM-printed PA6-CF15 composites. Optimized processing conditions not only improve interlayer adhesion but also modulate the damage morphology in a way that enhances shear resistance and energy dissipation during failure.

4. Conclusion

This study provides a comprehensive investigation into the shear strength and interlayer damage of short carbon fiber-reinforced PA6 composites produced by the FDM method, specifically focusing on the critical ZX build orientation. The key findings and contributions are summarized as follows.

- The experimental and numerical analyses clearly demonstrated the significant influence of FDM processing parameters on the mechanical performance and physical properties of PA6-CF15 composites. Higher nozzle temperatures (275 °C), minimal layer thickness (0.15 mm), increased outer wall counts (two walls), and moderate post-heat treatment (80 min) consistently yielded denser parts with lower surface roughness and superior shear strength. Conversely, suboptimal parameters, such as the absence of outer walls and lower thermal input, led to increased porosity, rougher surfaces, and reduced mechanical performance.
- While PA6-CF15 specimens generally exhibited higher maximum shear loads than pure PA6, their fracture behavior was more brittle, characterized by lower stroke values and limited plastic deformation. This distinct difference in ductility highlights a critical limitation in the ZX build orientation: the lack of effective fiber bridging between layers. SEM analysis confirmed that carbon fibers were primarily oriented within individual layers, failing to establish strong connections across interlayer boundaries, thus limiting the expected reinforcing effect in the Z-direction.
- The Taguchi experimental design proved highly effective in identifying optimal process parameters for maximizing shear strength. The determined optimal combination (A2B1C3D2: nozzle temperature of 260 °C, layer thickness of 0.15 mm, two outer walls, and 80 min of post-heat treatment) provides valuable guidance for manufacturing high-performance FDM-printed PA6-CF15 components. Layer thickness was identified as the most prominent factor, with increasing thickness detrimentally affecting shear strength.
- A comparison of the Rt and shear strength values indicates that smoother surfaces tend to yield better shear performance. For example, Experiment 7 had the lowest roughness (222.16 μm) and the highest shear strength (21.0 MPa), while Experiment 6 showed the opposite—highest roughness (678.44 μm) and one of the lowest strengths (9.7 MPa). This suggests that increased surface roughness at interlayer boundaries contributes to stress concentration and reduced bonding quality.
- The results indicate that layer thickness and wall line count significantly affect shear strength. Thinner layers promote better interlayer fusion by minimizing voids, while more outer walls enhance the structural integrity of the shear region. In contrast, nozzle temperature and heat treatment duration showed relatively limited effects due to constrained variation.
- Finite Element Analysis (FEA) successfully simulated stress distributions, revealing high stress concentrations near the shear notch regions, consistent with experimental failure observations. SEM images of fracture surfaces provided intricate details of damage morphologies, including fiber-matrix debonding, fiber pullout, matrix cracking, fiber breakage, and matrix smearing. The observations indicated that shear failure is predominantly governed by interfacial shear stress, and optimized processing conditions enhance both interlayer adhesion and the material's ability to dissipate energy during failure.

In summary, the findings underscore the necessity of carefully controlling printing parameters to mitigate the inherent anisotropic properties and weak interlayer bonding associated with additive manufacturing, thereby paving the way for the broader industrial application of these advanced materials. Future work could explore alternative fiber types, hybrid reinforcement strategies, and more advanced post-processing techniques to further enhance interlayer bonding and overall mechanical reliability.

Declaration of competing interest

The authors declare that they have no known competing financial interests or personal relationships that could have appeared to influence the work reported in this paper.

Acknowledgement

This study has been supported by the Recep Tayyip Erdoğan University Development Foundation (Grant Number: 02026007021626)

Murat Sarıkaya acknowledges the Polish National Agency for Academic Exchange (NAWA) under the Ulam Programme (Grant No. BPN/ULM/2023/1/00035).

References

[1] Wickramasinghe S, Do T, Tran P. FDM-based 3D printing of polymer and associated composite: a review on mechanical properties, defects and treatments. Polymers 2020;12. https://doi.org/10.3390/polym12071529.

[2] Maqsood N, Rimašauskas M, Ghobakhloo M, Mordas G, Skotnicová K. Additive manufacturing of continuous carbon fiber reinforced polymer composites using materials extrusion process. Mechanical properties, process parameters, fracture analysis, challenges, and future prospect. A review. Adv Compos Hybrid Mater 2024;7:202. https://doi.org/10.1007/s42114-024-01035-w.

[3] Adil S, Lazoglu I. A review on additive manufacturing of carbon fiber-reinforced polymers: current methods, materials, mechanical properties, applications and challenges. J Appl Polym Sci 2023;140:e53476. https://doi.org/10.1002/app.53476.

[4] Parandoush P, Lin D. A review on additive manufacturing of polymer-fiber composites. Compos Struct 2017;182:36–53. https://doi.org/10.1016/j.compstruct.2017.08.088.

[5] Saroia J, Wang Y, Wei Q, Lei M, Li X, Guo Y, et al. A review on 3D printed matrix polymer composites: its potential and future challenges. Int J Adv Des Manuf Technol 2020;106:1695–721. https://doi.org/10.1007/s00170-019-04534-z.

[6] Sun B, Mubarak S, Zhang G, Peng K, Hu X, Zhang Q, et al. Fused-deposition modeling 3D printing of short-cut carbon-fiber-reinforced PA6 composites for strengthening, toughening, and light weighting. Polymers 2023;15. https://doi.org/10.3390/polym15183722.
[7] Li X, He J, Hu Z, Ye X, Wang S, Zhao Y, et al. High strength carbon-fiber reinforced polyamide 6 composites additively manufactured by screw-based extrusion. Compos Sci Technol 2022;229:109707. https://doi.org/10.1016/j.compscitech.2022.109707.
[8] Peng X, Zhang M, Guo Z, Sang L, Hou W. Investigation of processing parameters on tensile performance for FDM-printed carbon fiber reinforced polyamide 6 composites. Compos Commun 2020;22:100478. https://doi.org/10.1016/j.coco.2020.100478.
[9] Al Rashid A, Ikram H, Koç M. Additive manufacturing and mechanical performance of carbon fiber reinforced Polyamide-6 composites. Mater Today Proc 2022;62:6359–63. https://doi.org/10.1016/j.matpr.2022.03.339.
[10] Cho B-G, Ram Joshi S, Hun Han J, Kim G-H, Park Y-B. Interphase strengthening of carbon fiber/polyamide 6 composites through mixture of sizing agent and reduced graphene oxide coating. Compos Part A Appl Sci Manuf 2021;149:106521. https://doi.org/10.1016/j.compositesa.2021.106521.
[11] Lupone F, Padovano E, Veca A, Franceschetti L, Badini C. Innovative processing route combining fused deposition modelling and laser writing for the manufacturing of multifunctional polyamide/carbon fiber composites. Mater Des 2020;193:108869. https://doi.org/10.1016/j.matdes.2020.108869.
[12] de Toro E, Coello Sobrino J, Martínez Martínez A, Miguel Eguía V, Ayllón Pérez J. Investigation of a short carbon fibre-reinforced polyamide and comparison of two manufacturing processes: Fused Deposition Modelling (FDM) and Polymer Injection Moulding (PIM). Materials 2020;13. https://doi.org/10.3390/ma13030672.
[13] Zhang R, Yu L, Chen K, Xue P, Jia M, Hua Z. Amelioration of interfacial properties for CGF/PA6 composites fabricated by ultrasound-assisted FDM 3D printing. Compos Commun 2023;39:101551. https://doi.org/10.1016/j.coco.2023.101551.
[14] Du H, Xian G, Tian J, Ma Z, Li C, Xin M, et al. Effect of fiber surface treatment with silane coupling agents and carbon nanotubes on mechanical properties of carbon fiber reinforced polyamide 6 composites. Polym Compos 2025;46:1267–83. https://doi.org/10.1002/pc.29035.
[15] Bai Y, Tian J, Li C, Wang J, Xian G. Experimental and numerical analysis of a new thermoplastic pultrusion technology of CF/PA6 rod using prepreg tapes. Polym Compos 2025. https://doi.org/10.1002/pc.29591. n/a.
[16] Li C, Xian G, Li H. Influence of immersion in water under hydraulic pressure on the interfacial shear strength of a unidirectional carbon/glass hybrid rod. Polym Test 2018;72:164–71. https://doi.org/10.1016/j.polymertesting.2018.10.004.
[17] Xian G, Guo R, Li C, Hong B. Effects of rod size and fiber hybrid mode on the interface shear strength of carbon/glass fiber composite rods exposed to freezing-thawing and outdoor environments. J Mater Res Technol 2021;14:2812–31. https://doi.org/10.1016/j.jmrt.2021.08.088.
[18] Xu Z, Zou B, Ding S, Zhuang Y, Wang X. Study on the hot isostatic pressing post-treatment of FDM-3D printed continuous carbon fiber reinforced composites. J Manuf Process 2023;104:205–17. https://doi.org/10.1016/j.jmapro.2023.08.060.
[19] Gupta Ashutosh Kumar, Krishnanand, Taufik Mohammad. Effect of process parameters on performances measured in filament and pellets-based additively manufactured parts. Proc Inst Mech Eng Part E J Process Mech Eng 2023;239:489–512. https://doi.org/10.1177/09544089231175207.
[20] Yadav A, Rohru P, Babbar A, Kumar R, Ranjan N, Chohan JS, et al. Fused filament fabrication: a state-of-the-art review of the technology, materials, properties and defects. Int J Interact Des Manuf 2023;17:2867–89. https://doi.org/10.1007/s12008-022-01026-5.
[21] Tran TQ, Ng FL, Kai JTY, Feih S, Nai MLS. Tensile strength enhancement of fused filament fabrication printed parts: a review of process improvement approaches and respective impact. Addit Manuf 2022;54:102724. https://doi.org/10.1016/j.addma.2022.102724.
[22] Wei Q, Yang R, Zhao X, Zhou J, An Y, Yang S. Fused deposition modeling of carbon-reinforced polymer matrix composites: a comprehensive review. Polym Compos 2023;44:5313–45. https://doi.org/10.1002/pc.27498.
[23] Karimi A, Rahmatabadi D, Baghani M. Direct pellet three-dimensional printing of polybutylene adipate-co-terephthalate for a greener future. Polymers 2024;16. https://doi.org/10.3390/polym16020267.
[24] Hasan MR, Davies IJ, Pramanik A, John M, Biswas WK. Impact of process parameters on improving the performance of 3D printed recycled polylactic acid (rPLA) components. Int J Adv Des Manuf Technol 2024;131:3751–79. https://doi.org/10.1007/s00170-024-13140-7.
[25] Orgeldinger C, Seynstahl A, Rosnitschek T, Tremmel S. Surface properties and tribological behavior of additively manufactured components: a systematic review. Lubricants 2023;11. https://doi.org/10.3390/lubricants11060257.
[26] Grzesik W. Prediction of the functional performance of machined components based on surface topography: state of the art. J Mater Eng Perform 2016;25:4460–8. https://doi.org/10.1007/s11665-016-2293-z.
[27] Zhao B, Song J, Xie L, Hu Z, Chen J. Surface roughness effect on fatigue strength of aluminum alloy using revised stress field intensity approach. Sci Rep 2021;11:19279. https://doi.org/10.1038/s41598-021-98858-0.
[28] Jipa A, Reiter L, Flatt RJ, Dillenburger B. Environmental stress cracking of 3D-printed polymers exposed to concrete. Addit Manuf 2022;58:103026. https://doi.org/10.1016/j.addma.2022.103026.
[29] Zhang Y, Zheng W, Wang Y, Ma K, Feng X, Ji Q, et al. A review of 3D printing continuous carbon fiber reinforced thermoplastic polymers: materials, processes, performance enhancement, and failure analysis. Polym Compos 2025. https://doi.org/10.1002/pc.29895. n/a.
[30] Hartomacıoğlu S, Kaya E, Eker B, Dağlı S, Sarıkaya M. Characterization, generative design, and fabrication of a carbon fiber-reinforced industrial robot gripper via additive manufacturing. J Mater Res Technol 2024;33:3714–27. https://doi.org/10.1016/j.jmrt.2024.10.064.
[31] Tiwary VK, A P, Malik VR. An overview on joining/welding as post-processing technique to circumvent the build volume limitation of an FDM-3D printer. Rapid Prototyp J 2021;27:808–21. https://doi.org/10.1108/RPJ-10-2020-0265.
[32] Singh S, Singh G, Prakash C, Ramakrishna S. Current status and future directions of fused filament fabrication. J Manuf Process 2020;55:288–306. https://doi.org/10.1016/j.jmapro.2020.04.049.
[33] Hartomacioğlu S. Optimization of production parameters for impact strength of 3D-Printed carbon/glass fiber-reinforced nylon composite in critical ZX printing orientation. Polymers 2024;16. https://doi.org/10.3390/polym16213006.
[34] Krajangsawasdi N, Blok LG, Hamerton I, Longana ML, Woods BKS, Ivanov DS. Fused deposition modelling of fibre reinforced polymer composites: a parametric review. J Compos Sci 2021;5. https://doi.org/10.3390/jcs5010029.
[35] Ismail KI, Yap TC, Ahmed R. 3D-Printed fiber-reinforced polymer composites by fused deposition modelling (FDM): fiber length and fiber implementation techniques. Polymers 2022;14. https://doi.org/10.3390/polym14214659.
[36] Patra AK, Ray I. Fracture behavior and toughness of fiber reinforced thermoset composites. In: Mavinkere Rangappa S, Satishkumar TP, Cuadrado MMM, Siengchin S, Barile C, editors. Fracture failure analysis of fiber reinforced polymer matrix composites. Singapore: Springer Singapore; 2021. p. 107–47. https://doi.org/10.1007/978-981-16-0642-7_6.
[37] Mohammadi R, Assaad M, Imran A, Fotouhi M. Fractographic analysis of damage mechanisms dominated by delamination in composite laminates: a comprehensive review. Polym Test 2024;134:108441. https://doi.org/10.1016/j.polymertesting.2024.108441.
[38] Qiao Y, Fring LD, Pallaka MR, Simmons KL. A review of the fabrication methods and mechanical behavior of continuous thermoplastic polymer fiber–thermoplastic polymer matrix composites. Polym Compos 2023;44:694–733. https://doi.org/10.1002/pc.27139.
[39] Liu W-H, Zhang L-W, Liew KM. Modeling of crack bridging and failure in heterogeneous composite materials: a damage-plastic multiphase model. J Mech Phys Solid 2020;143:104072. https://doi.org/10.1016/j.jmps.2020.104072.
[40] Shokrieh MM, Salamat-talab M, Heidari-Rarani M. Dependency of bridging traction of DCB composite specimen on interface fiber angle. Theor Appl Fract Mech 2017;90:22–32. https://doi.org/10.1016/j.tafmec.2017.02.009.
[41] Elhadary M, Hamdy A, Shaker W. Effect of fiber bridging in composites healing. Alex Eng J 2022;61:2769–74. https://doi.org/10.1016/j.aej.2021.08.002.